High-performance and Multi-functional Control of Transformerless Single-phase Smart Inverter for Grid-connected PV System

Kamran Zeb, Saif Ul Islam, Waqar Uddin, Imran Khan, Muhammad Ishfaq, Tiago Davi Curi Busarello, and H. J. Kim

Abstract—**Highly reliable and flexible control is required for distributed generation (DG) to efficiently connect to the grid. Smart inverters play a key role in the control and integration of DG into the power grid and provide advanced functionalities. In this paper, an energy-based single-phase voltage-source smart inverter (SPV-SSI) of 5 kVA is designed and analyzed in detail. SPV-SSI is capable of supplying the power to local load and the utility load up to the rated capacity of the inverter, injecting the power into the grid, storing the energy in lead-acid battery bank, controlling the voltage at the point of common coupling (PCC) during voltage sags or faults, and making decisions on real-time pricing information obtained from the utility grid through advanced metering. The complete design of smart inverter in *dq* frame, bi-directional DC-DC buck-boost converter, IEEE standard 1547 based islanding and recloser, and static synchronous compensator (STATCOM) functionalities is presented in this paper. Moreover, adaptive controllers, i.e., fuzzy proportional-integral (F-PI) controller and fuzzy-sliding mode controller (F-SMC) are designed. The performances of F-PI controller and F-SMC are superior, stable, and robust compared with those of conventionally tuned PI controllers for voltage control loop (islanded mode) and current control loop (grid-connected mode).**

Index Terms—**Distributed generation (DG), inverter, converter, fuzzy-sliding mode controller (F-SMC), fuzzy proportional-integral (F-PI) controller.**

I. Introduction

DECLINING fossil fuel resources and worldwide environmental problems deepen the urgency of transitioning in the direction of sustainable energy resources [1]. In the last few decades, the installation of solar photovoltaic (PV) energy is flourishing at a fast rate among various renewable energy sources (RESs). As a result, global installation capacity of SPV approaches 405 GW. It is forecasted that in 2020, the installation capacity of PV (772 GW) will exceed that of wind energy (735 GW) [2]. Recently, advance grid functionalities (AGFs) are added into the standard of distributed generation units (DGUs) which are connected to the power grid due to the progressing penetration of DG. The aim of these functionalities is to support the power grid during fluctuations and faults. Some examples of AGFs anticipated by the modified standard are reactive power generation, low- or high-voltage ride through capability, and low- or high-frequency ride through capability [3].

Smart inverters (SIs) play a key role in the control and integration of DG to the power grid [4]. Apart from its main function of DC power conversion to AC power, it has multiple functions including frequency control, fault ride through, ramp-rate control, active power control, power factor control and voltage regulation, etc. Currently, different countries demonstrate real distribution and transmission systems to motivate their rapid deployment [5].

Single-phase voltage-SIs (SPV-SIs) are widely used in DGU owing to its promising features of bi-directional energy flow competency, low-current harmonics, and high-power factor [6]. To efficiently inject the generated power from the PV, various researches have concentrated on grid-tied inverters. The topics include controller design, control strategies, and inverter topologies, etc. [7]. Various controllers are scrutinized in order to control transient-state and steady-state performances of grid-connected PVs, i.e., sliding mode controller (SMC) [8], proportional-resonant (PR) controller [9], deadbeat controller [10], hysteresis controller [11], repetitive controller, and grid voltage feedforward based proportional-integral (PI) controller [12]. Furthermore, neural networks, adaptive controller, artificial intelligence methods based on fuzzy logic, and neuro-fuzzy are also proposed in [13]-[16]. Similarly, in terms of transient response and steady-state error, the preferences and drawbacks of these strategies have been designed in literature.

The Smart Grid Initiative (SGI) has been approved as an official policy by the US government to modernize the power grid. The motive of SGI is to boost up the integration of

Manuscript received: May 16, 2019; accepted: May 15, 2020. Date of CrossCheck: May 15, 2020. Date of online publication: September 24, 2020.

This work was supported by Creative Human Resource Development Program (No. BK21PLUS).

K. Zeb (corresponding author), S. U. Islam, W. Uddin, I. Khan, M. Ishfaq, and H. J. Kim are with the Department of Electrical Engineering, Pusan National University, San 30, South Korea, and K. Zeb is also with the School of Electrical Engineering and Computer Science, National University of Sciences and Technology, Islamabad, Pakistan (e-mail: kami_zeb@yahoo. com; engr. saifulislam19@gmail. com; waqudn@pusan. ac. kr; imrankhan@pusan. ac. kr; engrishfaq1994@gmail.com; heeje@pusan.ac.kr).

T. D. C. Busarello is with the Department of Control, Automation and Computing Engineering, Federal University of Santa Catarina Blumenau, Rua João Pessoa, Brazil (e-mail: tiago.busarello@ufsc.br).

DOI: 10.35833/MPCE.2019.000331

RESs into the power grid, the installation of advanced technologies, real-time electricity pricing and metering [17]. The design of power electronics based SIs is one of the main goal of SGI.

In this paper, SGI based SPV-source smart inverter (SPV-SSI) is designed and analyzed with combined capability as follows: supplying the power to local load; injecting the power into the power grid; supplying the power to the utility load up to the nominal capacity of the inverter; storing the energy in lead-acid battery bank; controlling the voltage at the point of common coupling (PCC) during voltage faults/sags; and decision making on real-time pricing information acquired from the utility grid via advanced metering. Additionally, fuzzy PI (F-PI) controller and F-SMC are designed to overcome the deficiencies of the conventionally-tuned PI controller. The F-PI controller integrates the advantages of a traditional PI and fuzzy logic controller (FLC). It exhibits faster and better dynamic response, easy implementation, less updated parameters, and zero steady-state error [14]. In F-SMC, two nonlinear control techniques such as F-PI and SMC are combined in a single controller. F-PI minimizes the chattering under the steady-state conditions. The transient state error is reduced by SMC, offering a fast dynamic response and system stability [12]. SMC is also insensitive to parameter uncertainties and load disturbances.

The contributions of this paper are listed as follows.

1) dq implementation of the SI and $T/4$ delay based single-phase phase lock loop (PLL) structure.

2) Design of voltage control loop for stand-alone operation and current control loop for grid-connected operation.

3) Efficient design of bi-directional DC-DC buck-boost converter (BDC-DCBBC), static synchronous compensator (STATCOM) capability, and IEEE standard 1547 based islanding and re-closer functionalities.

4) Design of robust and adaptive controllers, i.e., F-PI controller and F-SMC for voltage and current control loops.

5) Comparative analysis of designed controllers with traditionally-tuned PI controllers under various conditions.

6) Effectively operating SI in stand-alone mode, grid-connected mode, and various submodes in each supermode.

The remainder of this paper is organized as follows. Section II presents the mathematical modelling of inverter and the design of control loops. System description along with smart functionalities are elaborated in Section III. Section IV describes the design controllers. Performances are evaluated in Section V. Finally, Section VI concludes the paper.

II. Mathematical Modelling

A. Single-phase Inverter dq Implementation

The control is designed in the dq-rotating reference frame. Two orthogonal components with virtual q-axis are created from single-phase quantities. Two methods are used to obtain the virtual component, i.e., delaying the real component by 1/4 of its own period or derivating the fundamental signal [17]. The derivative method is presented by (1)-(4).

The required output signal of the inverter is presented as:

$$x_\alpha(t) = A_\alpha \cos(\omega t + \phi) \tag{1}$$

where x_α is the required output signal of the inverter; A_α is the signal amplitude; ω is the fundamental frequency of output voltage; and ϕ is the phase angle of the initial system.

$$x_\beta = \frac{\mathrm{d}}{\mathrm{d}x} x_\alpha(t) \tag{2}$$

where x_β is the first derivative of the output equation; and x is the variable (current or voltage).

$$x_\beta = A_\beta \sin(\omega t + \phi) \tag{3}$$

where A_β is the amplitude of imaginary system. After taking the derivative of $x_\alpha(t)$, A_β becomes:

$$A_\beta = -\omega A_\alpha \tag{4}$$

In this paper, delaying the real component by 1/4 of its own period is used in order to acquire the imaginary system. $T/4$ delay based single-phase PLL structure is shown in Fig. 1, where V_α, V_β, V_d, V_q are the voltage of α, β, d, q axes, respectively; and ω_0 is the initial fundamental frequency of output voltage. For $\alpha\beta \rightarrow dq$ transformation, (5) is used as:

$$\begin{bmatrix} X_d \\ X_q \end{bmatrix} = \begin{bmatrix} \cos(\omega t) & \sin(\omega t) \\ -\sin(\omega t) & \cos(\omega t) \end{bmatrix} \begin{bmatrix} x_\alpha \\ x_\beta \end{bmatrix} \tag{5}$$

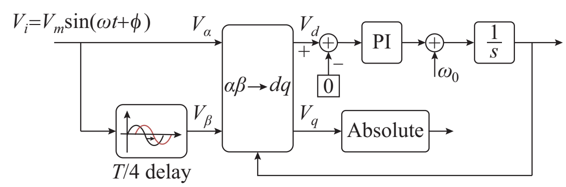

Fig. 1. $T/4$ delay based single-phase PLL structure.

B. Voltage and Current Control Loops

The inverter operates in voltage control loop and current control loop. The structure of designed current and voltage control is presented in Fig. 2 [17]. The voltage control loop is for a stand-alone inverter and the current control loop is for a grid-connected inverter. The detailed description of the inverter is discussed in Section III. In this paper, we only focus on control loop implementation. The information of phase angle and frequency is supplied by PLL [12]. The sinusoidal pulse width modulation (SPWM) modulator references are generated by PI controllers.

$$A_{ref} = \sqrt{D^2 + Q^2} \tag{6}$$

$$\phi_{ref} = \alpha\tan(g)\frac{Q}{D} \tag{7}$$

where A_{ref} is the sinusoidal amplitude; ϕ_{ref} is the phase angle references; and D and Q are the corresponding values of d-axis and q-axis, respectively. V_{dref} is set to be 1 and V_{qref} is set to be 0 as reference voltage. The current references I_{dref} and I_{qref} are calculated from active and reactive reference power, i.e., P_{ref} and Q_{ref} using (5) and (8) to (10) for the current loop. The calculated currents are compared with the output line currents which are previously converted to dq reference frame. By applying PI controller, the error is minimized in order to generate required sinusoidal reference for SPWM modulator.

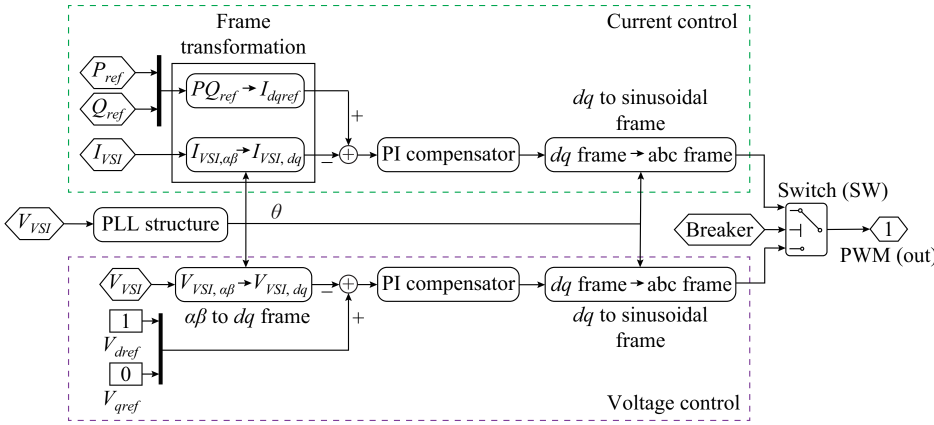

Fig. 2. Structure of designed current and voltage control.

$$A = \frac{\sqrt{P_{PU}^2 + Q_{PU}^2}}{V_{2PU}} \tag{8}$$

$$\phi_{I_{ref}} = \alpha \tan(g) \frac{Q_{PU}}{P_{PU}} \tag{9}$$

$$I_{ref}(t) = A_{I_{ref}} \sin(\omega t + \phi_{I_{ref}}) \tag{10}$$

where $A_{I_{ref}}$ is the reference current amplitude; I_{ref} is the sinusoidal value of reference current; $\phi_{I_{ref}}$ is the phase angle of reference current; P_{PU} and Q_{PU} are the active and reactive components of the power, respectively; and V_{2PU} is the local load voltage. From PLL of voltage V_{2PU}, the angle ωt is acquired at the LCL filter output.

III. System Description and Smart Functionalities

SPV-SSI has the capacity of 5 kVA, the operation voltage of 120 V, and the frequency of 60 Hz. All nominal parameters are listed in Table I. The inverter operates in dual control loops, and the proposed model of SPV-SSI is shown in Fig. 3. The voltage control loop is used for stand-alone operation and the current control loop is used for grid-connected operation [17].

TABLE I
System Specification

Parameter	Value
Capacity	5 kVA
DC-link voltage V_{dc}	350 V
Full-bridge converter voltage	120 V
Nominal frequency	60 Hz
Filter inductor L_1	300 μH
Filter capacitor C	13.6 μF
Filter inductor L_2	300 μH

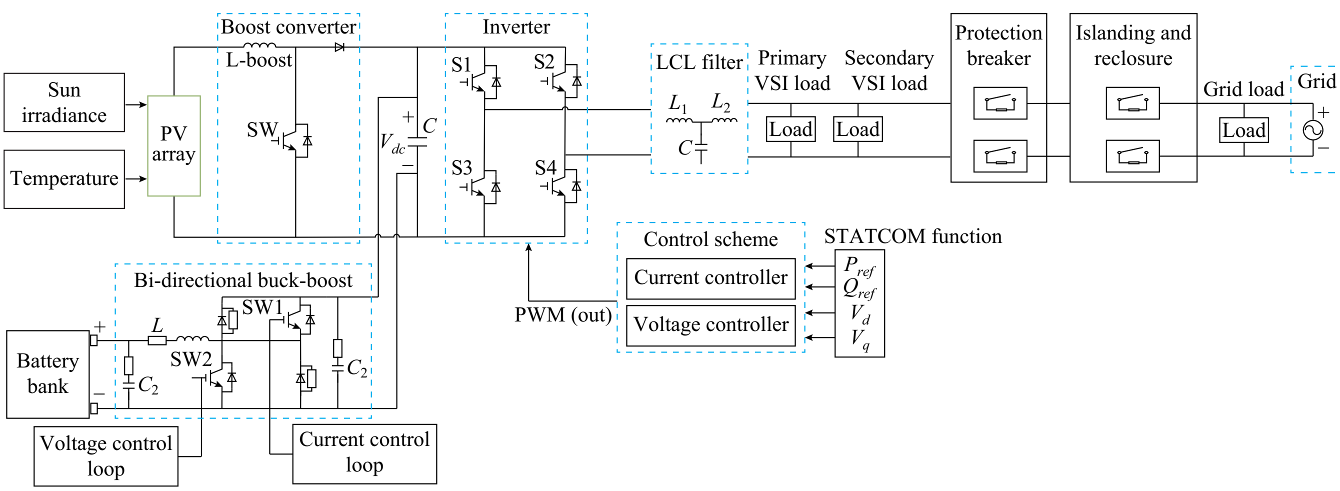

Fig. 3. Proposed model of SPV-SSI.

The dq frame with a virtual q-axis is used for the implementation of the entire control. The phase information to the control loops is supplied by PLL. Four PI controllers are used for the voltage and the current controllers, i.e., two PI controllers for V_d and V_q and two for I_d and I_q. The input to the inverter is supplied by PV panels with a rated voltage of 192 V and a steady-state voltage of 350 V. The DC-link voltage is maintained at 350 V by the DC-DC boost converter. As presented in Fig. 3, BDC-DCBBC is also connected with lead-acid battery storage of 24 Ah cell and a nominal voltage of 192 V. The battery design is taken from [18], and the advantages of the storage system are: when the system is in islanded mode, the stored energy can be used to supply local loads, sell the electricity when the price is high, and store cheap energy. Additionally, each block of the model is implemented as follows.

A. BDC-DCBBC

The charging and discharging of the battery system are controlled by BDC-DCBBC, whose specification is given in Table II.

TABLE II
NOMINAL PARAMETERS OF BDC-DCBBC

Parameter	Value
Power P	5 kW
Switching frequency f_{sw}	15 kHz
Battery voltage V_B	192 V
DC-link voltage V_{dc}	350 V
Inductor resistance r_L	0.02 Ω
Battery bank resistance r_B	0.2 Ω
C_1 and C_2 resistance r_C	0.05 Ω

When SW1 is ON, the converter is in buck mode and the battery is charging. And for boost mode, SW2 is ON and the battery is discharging. For the operation in buck mode, the average current method based current control loop is designed. The K factor-based voltage control loop is designed for boost operation [17]. The nominal inductor current I_L for the buck-boost is calculated as:

$$I_L = \frac{P}{V_B} \tag{11}$$

The value of the inductor is designed by (12). L limits the DC-link ripple current to 50% of I_L.

$$L = \frac{V_B(V_{dc} - V_B)}{f_s V_{dc} \times 0.5 \times I_L} \tag{12}$$

$$C_1 = \frac{0.5 I_L}{8 f_s \times 0.001 \times V_B} \tag{13}$$

Similarly, the boost capacitor C_2 is designed in (14). The DC-link ripple voltage is limited to 0.1% of V_{dc}.

$$C_2 = \frac{P(V_{dc} - V_B)}{f_s \times 0.001 \times V_{dc}^3} \tag{14}$$

1) Current Control Loop

For the current control loop of BDC-DCBBC, the type 2 controller of buck-boost converter is used whose transfer function is $G_2(s)$ [17] and is given as:

$$G_2(s) = \frac{K_2(s+\omega_z)}{s(s+\omega_P)} \tag{15}$$

where K_2 is the DC gain of type 2 controller; $\omega_P = \omega_{GC}\sqrt{K}$, ω_{GC} is the zero-crossing gain frequency, and K is the constant designed from boost phase advance; and $\omega_z = \omega_{GC}/\sqrt{K}$.

2) Voltage Control Loop

The transfer function of small-signal dynamic boost model is given by the following equation [17].

$$T_{boost}(s) = \frac{-1.3\times10^{-4}s^2 + 0.22s + 3.5\times10^4}{9.4\times10^{-5}s^2 + 1.3\times10^{-2}s + 47.2} \tag{16}$$

For voltage control loop of BDC-DCBBC, the type 2 controller is used whose transfer function is $G_3(s)$ [17] and is:

$$G_3(s) = \frac{K_3(s+\omega_z)(s+\omega_z)}{s(s+\omega_P)(s+\omega_P)} \tag{17}$$

where K_3 is the type 3 DC gain.

B. STATCOM, Islanding and Recloser Capability

As confirmed in [5], [19], to regulate the reactive power by individual DG system (SPV), it can also be used to offer voltage support at low-voltage distribution. STATCOM is a power electronics based voltage-source converter that works either as a sink or source of reactive power. To control the voltage at PCC, the reactive power should be injected into the AC grid. Therefore, the inverter in DG systems must be connected with STATCOM. In order to inject reactive power for voltage compensation, the voltage sag at the grid side is calculated from the nominal voltage magnitude and grid voltage magnitude. The sag voltage is kept null by the PI compensator. Based on IEEE standard 1547, it is capable for the converter to connect and island to (and from) the grid islanding and recloser functionalities.

IV. CONTROLLER DESIGN

A. Design of F-PI Controller

The proportional gain K_p and integral gain K_i of simple PI control are constant. The PI controller fails to work effectively when an external or internal disturbance occurs in the system. Therefore, the gains require the adaptation according to the error $e(t)$ to enhance the performance of the PI control scheme. In this paper, fuzzy rules (FRs) are used to update the PI gains.

The design of the F-PI controller is illustrated in Fig. 4 [20]. FRs are simple if-then statements, which generates the conclusion based on conditions in [12], [20]. For controlling the output of the controller, the following FRs are used as shown in Table III.

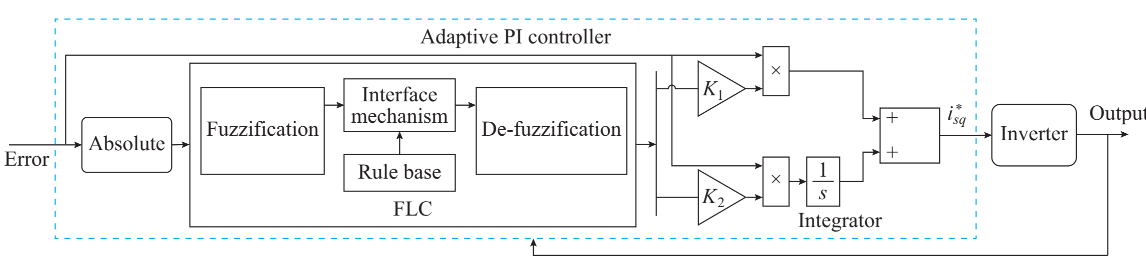

Fig. 4. Design of F-PI controller.

TABLE III
FRs

No.	If-then rules		Input membership function		Output membership function	
	If $\lvert e(t) \rvert$	Then (K_p, K_i)	Linguistic term	Range	Linguistic term	Range
1	Large	Large	Large	[0.7, 1.0]	Large	[0.7, 1.0]
2	Small	Small	Small	[0.3, 0.8]	Small	[0.3, 0.8]
3	Zero	Zero	Zero	[0, 0.2]	Zero	[0, 0.2]

The membership function used in fuzzification and defuzzification steps is triangular membership function (TMF) to map crisp/real input into fuzzy output and vice versa. TMF is given as:

$$\mu_A(x)=\begin{cases} 0 & x\le a, x\ge b \\ \dfrac{x-a}{m-a} & a<x\le m \\ \dfrac{b-x}{b-m} & m<x<b \end{cases} \tag{18}$$

where a is the lower limit; b is the upper limit; and m is the peak value of TMF. In addition, $a<m<b$. Mathematically, the output of a simple PI controller is represented as:

$$\frac{V_{dq}}{I_{dq}}=K_p e(t)+K_i\int e(t)\,\mathrm{d}t \tag{19}$$

In the above equation, the output of the current controller for grid-connected mode is I_{dq} and that of the voltage controller for islanded mode is V_{dq}.

In the F-PI controller, by using FR, the PI gains are updated in order to minimize the errors. Equation (20) presents the output equation of the designed fuzzy controller.

$$\frac{V_{dq}}{I_{dq}}=F_1K_1e(t)+F_2K_2\int e(t)\,\mathrm{d}t \tag{20}$$

where K_1 and K_2 are the learning rate gains for K_p and K_i, respectively; and F_1 and F_2 are the outputs of the fuzzy controller for K_p and K_i, respectively. Figure 4 demonstrates the implementation of the output equation.

B. Design of F-SMC

In F-SMC, two adaptive nonlinear approaches are used to update the designed controller, i. e., F-PI controller and SMC. F-SMC has the dominant features of F-PI controller and SMC [20]. The transient-state error is minimized by SMC. Thus, the quick dynamic response is ensured and the system stability is enhanced. In steady state, the chattering reduced by F-PI controller and F-SMC is presented in Fig. 5.

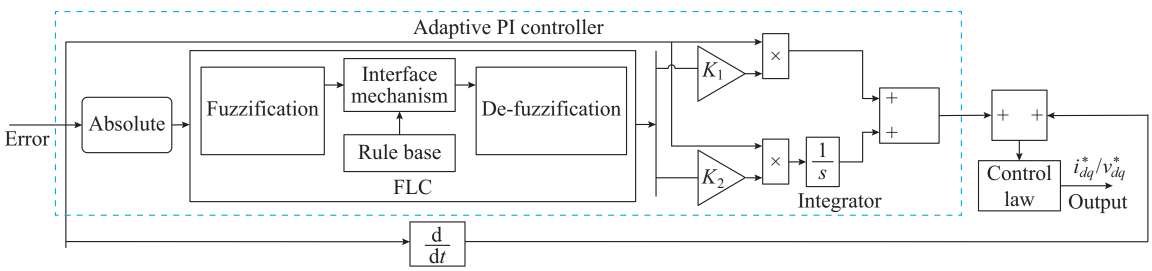

Fig. 5. Chattering reduced by F-PI controller and F-SMC.

FRs are used to update gains K_p and K_i for sliding surface (SS). Besides, SS updated by F-PI controller control law is designed. The control law is based on a continuous smooth approximation [12], [20]. SMC error and its derivative will always be directed towards SS. The error and its derivative define SS $S(t)$ as:

$$S(t)=\dot{e}(t)+\lambda e(t) \tag{21}$$

where λ is the bandwidth dependent and an arbitrary constant. Besides, $\lambda e(t)$ is defined as:

$$\lambda e(t)=F_1K_1e(t)+F_2K_2\int e(t)\mathrm{d}t \tag{22}$$

The F-PI controller is used to update the value of $\lambda e(t)$. The control law for SS based on a discontinuous function is:

$$\frac{V_{dq}}{I_{dq}}=-Usgn(S) \tag{23}$$

where U is the bulky positive constant; and $sgn(S)=U$ when $S>0$ and $sgn(S)=-U$ when $S<0$. PWM control signals are employed in the electrical system and the discontinuous control law (23) causes the oscillation. Alternatively, a continuous smooth estimation based control law is designed which minimizes the chattering phenomena and is presented in (24).

$$\frac{V_{dq}}{I_{dq}}=-Usat(\sigma;\varepsilon)=\left[-U\frac{S}{|S|+\varepsilon}\right] \quad \varepsilon>0, \varepsilon\approx 0 \tag{24}$$

where $Usat(\sigma;\varepsilon)=U$ when $(\sigma;\varepsilon)>0$ and $Usat(\sigma;\varepsilon)=-U$ when $(\sigma;\varepsilon)<0$. In addition, the constants of both controllers are presented in Table IV.

TABLE IV
CONTROL SCHEME CONSTANT

Control strategy	Voltage control loop		Current control loop	
	Parameter	Value	Parameter	Value
PI	K_p	0.20	K_p	0.70
	K_i	45.00	K_i	150.00
F-PI	K_1	2.00	K_1	0.50
	K_2	130.00	K_2	0.75
F-SMC	K_1	2.50	K_1	2.00
	K_2	350.00	K_2	270.00
	ε	0.55	ε	0.50

V. Results and Discussions

In this section, all the possible premises of the operation of the designed SPV-SSI are discussed and described along with the validation of three case studies. The test bench is discussed in Section III. Based on the smart functionalities, the designed inverter operates in two modes: supermode and submode. The supermode is further categorized into stand-alone M_1 and grid-connected M_2 according to the compliance with IEEE standard 1547. M_1 is further divided into three submodes m_1, m_2, m_3 (M_1m_1, M_1m_2, M_1m_3) depending on P_{inv} and Z_{inv}, where P_{inv} is equal to total input power (PV panels plus battery bank) and Z_{inv} is equal to total load (primary VSI plus secondary VSI loads). In mode M_1m_1, P_{inv} is less than Z_{inv}, the demand is greater than the supply. In such case, the prioritization of loads occurs. Secondary VSI load is disconnected and the inverter supplies power to the other primary load. The remaining (excess) power is stored in the battery. As presented in Table V, mode M_1m_2 is simple. In mode M_1m_3, the inverter either supplies or stores the energy if required.

TABLE V
Stand-alone Modes

Mode	Functionality
M_1m_1	$P_{inv}<Z_{in}$, then supply to primary L and the remaining power for battery bank
M_1m_2	$P_{inv}>Z_{inv}$, then supply to Z_{inv} and excess power for battery bank
M_1m_3	$P_{inv}=Z_{inv}$, then supply to load or prioritization for later use

In mode M_2, the inverter operates in the following submodes M_2m_1, M_2m_2, and M_2m_3 depending on active and reactive power trading for economic consideration of spot-pricing P_{inv} and Z_{inv}. The economic consideration variables are the price of selling active power P_S, the price of selling reactive power Q_S, and a threshold value of electricity unit price from the power grid. The submodes are explained in Table VI.

TABLE VI
Grid-connected Modes

Mode	Functionality
M_2m_1	$Q_S \geq P_S$, then the inverter is controlled to supply voltage support compensation to the grid
M_2m_2	$Q_S \leq P_S$, then the inverter is controlled to bring the reactive power reference to null and deliver real power to local loads Z_{inv} and the excess to battery bank or grid
M_2m_3	Grid electricity price is less than marginal cost of electricity Power is supplied by the grid and P_{inv} is stored in the battery for later use Grid electricity price is more than marginal cost of electricity, then Z_{inv} is supplied by P_{inv}. The remaining energy is stored in battery or sold to the grid

In mode M_2m_1, $Q_S \geq P_S$ and the inverter offers voltage support compensation to the power grid. In mode M_2m_2, $Q_S \leq P_S$ and the inverter supplies real power to Z_{inv} and sets the reference of reactive power to zero. Extra active power is stored in a battery bank or sold to the power grid. Mode M_2m_3 is based on the options of using inverter power against purchasing the power from the power grid in case of non-availability of DG power.

A. Mode M_1m_1

In this mode, primary VSI and secondary VSI loads are 4 kW and 2 kW, respectively. The panel power is set to be 3 kW while the battery power is set to be 2 kW. At 0.3 s, the inverter operates in grid-connected mode and after 0.3 s, the grid is disconnected due to a fault in the grid. In stand-alone mode, the PV panels are unable to supply the power to the load, thus the battery in the boost mode is also active to supply the power to the load.

Figure 6 presents the active and reactive power at the inverter and grid sides. Since the total load is 6 kW, 5 kW is supplied by an inverter (3 kW from the PV panels and 2 kW from the battery) and 1 kW from the power grid.

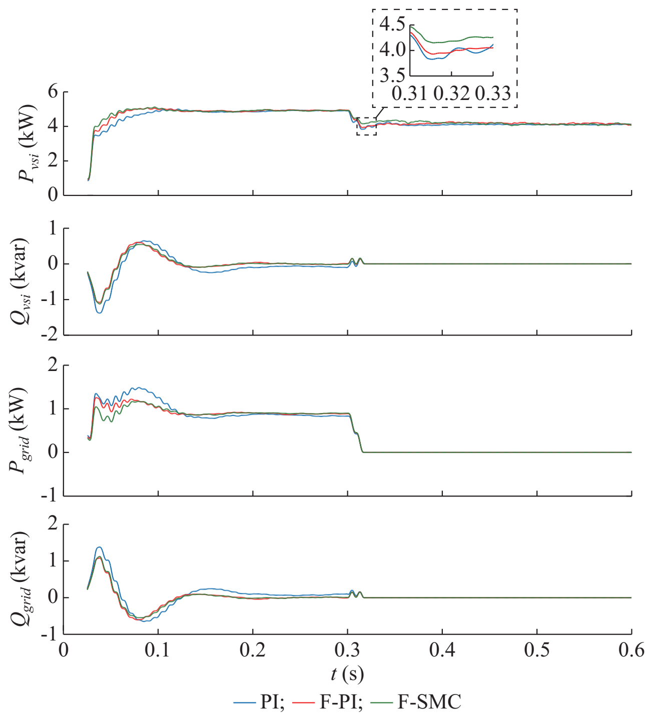

Fig. 6. Active and reactive power at inverter and grid sides in mode M_1m_1.

In addition, the reactive power is set to be 0. As the power grid is disconnected, the load is 6 kW and the inverter can supply a maximum 5 kW. Therefore, the secondary load (2 kW) is disconnected and the inverter supplies to the primary load (3 kW from panels and 1 kW from the battery). Furthermore, the responses of F-PI controller and F-SMC are robust, faster, and have less chattering compared with PI controller. Besides, more sensitivity is noticed for disturbances of PI controller system.

The voltage and current at the inverter and grid sides for PI controller, F-PI controller, and F-SMC are depicted in Fig. 7. The voltage and current of the inverter at 0.3 s is 1 p.u., specifying that the active power at the inverter side is 5 kW (2 kW from the battery bank and 3 kW from the PV panels). The voltage at the grid side is 1 p.u., but the current at the grid side is 0.2 p.u., signifying that the power at the grid side is 1 kW. After 0.3 s, the power grid is disconnected and the current approaches to 0. The current at inverter side is

0.8 as the secondary load is disconnected. Compared with F-PI controller and F-SMC, at the inverter side, the current and voltage take some time to be in phase initially as well as at 0.3 s when the power grid is disconnected. Similarly, at the grid side, when the power grid is disconnected, the grid voltage increases to 1.2 p.u. by using PI controller, and it is in the limit by using F-PI controller and F-SMC.

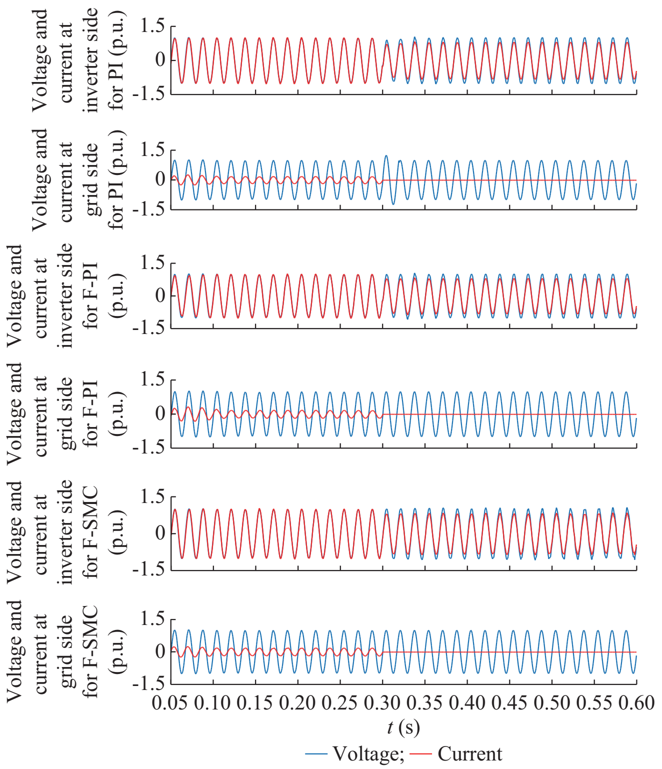

Fig. 7. Voltage and current at inverter and grid sides for PI controller, F-PI controller, and F-SMC in mode M_1m_1.

B. Mode M_2m_1

In mode M_2m_1, $Q_S \geq P_S$ and the inverter offers voltage support compensation to the power grid. Both the inverter loads, i.e., primary and secondary loads are set to be 1 kW. A voltage sag is introduced from 1 s to 1.7 s. By utilizing the STATCOM capability of the inverter, the voltage at the grid side is 1 p.u.. The active and reactive power at the inverter and grid sides for mode M_2m_1 are presented in Fig. 8. At $t=1$ s, the active power at the inverter side is 5 kW, while the active power at the grid side is −3 kW as 2 kW is used by the inverter load. During voltage sag from 1 s to 1.7 s, active and reactive power at the grid side are 4.2 kW and 2.7 kvar, respectively. Besides, the active and reactive power at the grid side are −2.2 kW and −2.7 kvar, respectively. This means that the power grid is purchasing active power as well as reactive power from the inverter, which supplies reactive power to compensate the voltage sag. When the sag is cleared, the original values are retained. Additionally, voltage and current at the inverter and grid sides for PI controller, F-PI controller, and F-SMC are presented in Fig. 9. At $t=$ 1 s, both the current and voltage at the inverter side are 1 p.u. while the voltage at the grid side is 1 p.u. and the current is 0.6 p.u.. During the voltage sag, the current and voltage at the inverter side are 1 p.u. with 32.4° of phase difference. The zoom part clearly shows that the response of designed controllers is stable, faster and robust compared with that of the PI controller. The PI controller is sensitive to sudden variation; whereas F-SMC is insensitive to sudden disturbances; and F-PI controller is less sensitivity. The designed controllers are faster, robust, and efficient.

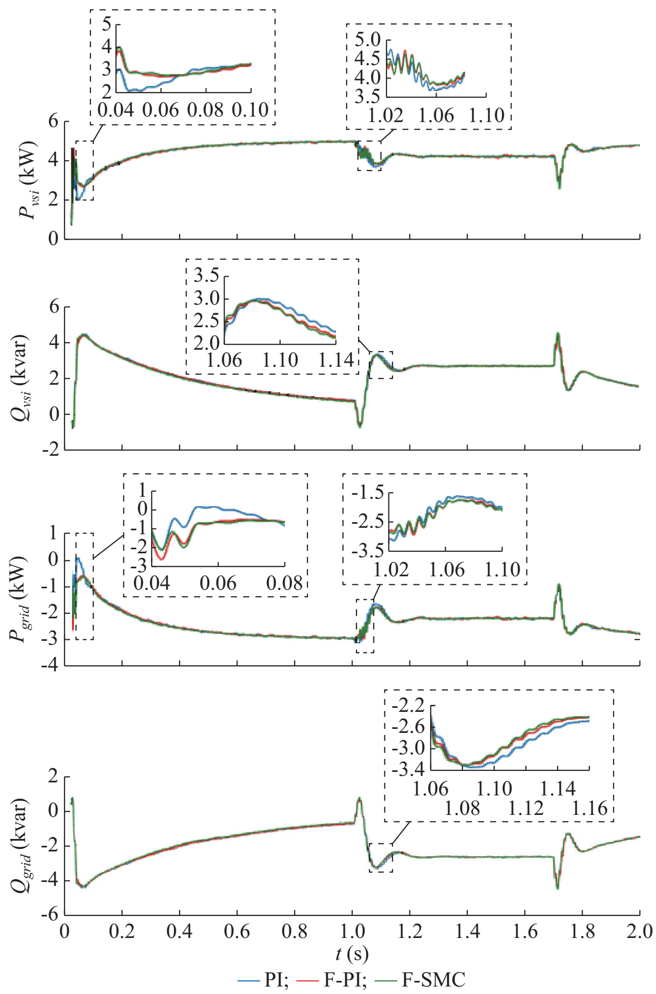

Fig. 8. Active and reactive power at inverter and grid sides in mode M_2m_1.

C. Mode M_2m_3

Mode M_2m_3 is based on the options of using inverter power against purchasing power from the power grid in the event of DG power availability. In this case, the primary and secondary loads of the inverter are set to be 3 kW and 2 kW, respectively. The set marginal preference MCP (2 \$/kW) is greater than the real-time grid electricity price P_B (1 \$/kW). The active power of the power grid is bought to feed the primary and secondary loads as well as charge the battery bank. The buck mode switch is ON for the bi-directional boost converter. Figure 10 presents the active and reactive power at the inverter and grid sides. The active power of the inverter is −5 kW, indicating that the inverter is purchasing the power because it is cheaper.

The PI controller exhibits large variation, slower response, long settling time, and high chattering compared with those of designed F-PI controller and F-SMC.

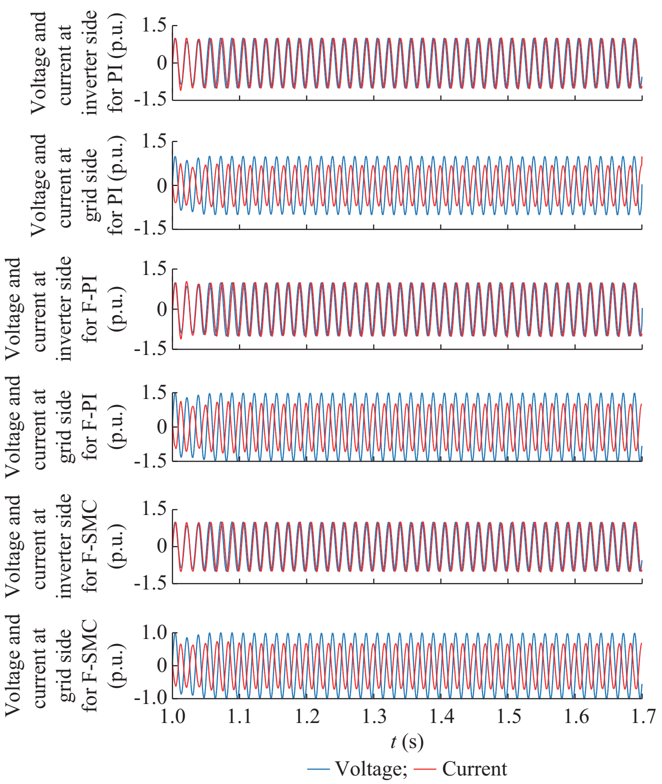

Fig. 9. Voltage and current at inverter and grid sides for PI, F-PI, and F-SMC in mode M_2m_3.

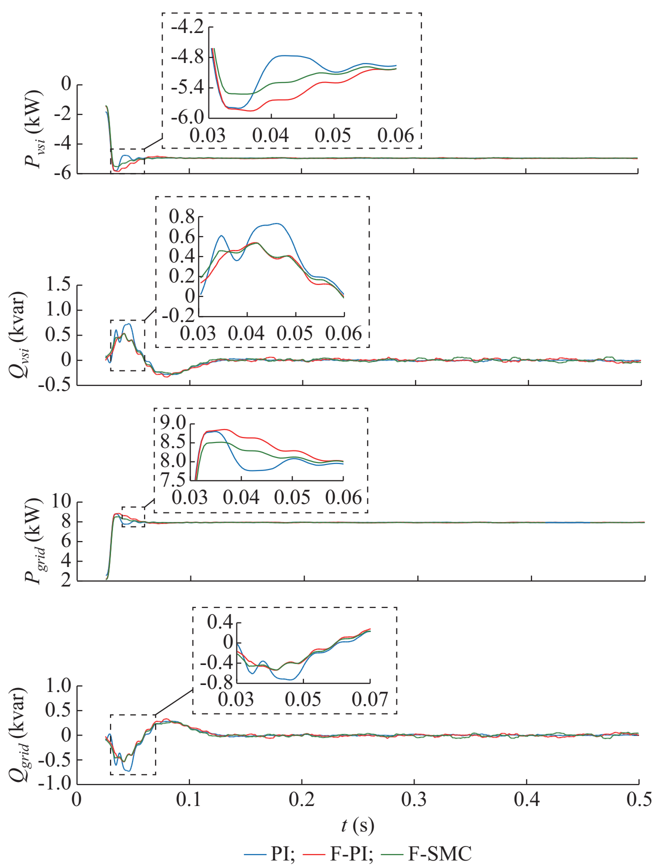

Fig. 10. Active and reactive power at inverter and grid sides for in mode M_2m_3.

The reactive power demands of the inverter load are set to be 0. The active power at the grid side is 8 kW, indicating that the grid is selling the active power. In addition, the responses of F-PI controller and F-SMC are robust and faster.

VI. Conclusion

In this paper, energy-based 5 kVA SPV-SSI is successfully designed, analyzed, and validated. The designed inverter not only injects active and reactive power but also provides voltage support at PCC during voltage sags/swells. In addition, it also stores surplus energy in lead-acid battery bank and efficiently decides whether to sell or purchase the power to or from the grid based on real-time information through advanced metering. Moreover, a complete design of SI in *dq* frame, BDC-DCBBC, IEEE standard 1547 based islanding and recloser, and STATCOM functionalities is also discussed. The simulation results for different cases are verified. The performances of F-PI controller and F-SMC are superior, stable, and robust compared with those of conventionally tuned PI controllers both for voltage control loop and current control loop. The dynamic and steady-state performances of the SPV-SSI are enhanced by designed controllers, and the power increases to a great extent. The quality of the voltage and current at the grid side is also refined. Besides, the proposed controller is less sensitive to sudden disturbances, and it exhibits fast dynamic response, low-voltage dips, less oscillations and chattering, and fault-tolerant capability compared with those of the fine-tuned PI controller.

References

[1] F. Blaabjerg, Z. Chen, and S. B. Kjaer, "Power electronics as efficient interface in dispersed power generation systems," *IEEE Transactions on Power Electronics*, vol. 19, no. 5, pp. 1184-1194, Sept. 2004.

[2] K. Zeb, I. Khan, W. Uddin *et al.*, "A review on recent advances and future trends of transformerless inverter structures for single-phase grid-connected photovoltaic systems," *Energies*, vol. 11, no. 8, p.1968, Jul. 2018.

[3] IEC, "Advanced functions for DER inverters," International Electrotechnical Commission, Tech. Rep. TR-IEC 61850-90-7, Jan. 2012.

[4] EPRI, "Common functions for smart inverters," Electric Power Research Institute, Palo Alto, USA, Feb. 2016.

[5] T. Stetz, F. Marten, and M. Braun, "Improved low voltage grid-integration of photovoltaic systems in Germany," *IEEE Transactions on Sustainable Energy*, vol. 4, no. 2, pp. 534-542, Apr. 2013.

[6] F. Evran, "Plug-in repetitive control of single-phase grid-connected inverter for AC module applications," *IET Power Electronics*, vol. 10, no. 1, pp. 47-58, Jan. 2017.

[7] C. Krismadinata, N. A. Rahim, and J. Selvaraj, "Implementation of hysteresis current control for single-phase grid connected inverter," in *Proceedings of International Conference on Power Electronics Drive Systems*, Bangkok, Thailand, Nov. 2007, pp. 1097-1101.

[8] F. Fuchs, J. Dannehl, and F. W. Fuchs, "Discrete sliding mode current control of grid-connected three-phase PWM converters with LCL filter," in *Proceedings of IEEE International Symposum Industrial Electronics*, Barcelona, Spain, Aug. 2010, pp. 779-785.

[9] G. Shen, X. Zhu, J. Zhang *et al.,* "A new feedback method for PR current control of LCL-filter-based grid-connected-inverter," *IEEE Transactions on Industrial Electronics*, vol. 57, no. 6, pp. 2033-2041, Jun. 2010.

[10] T. Ahmed, K. Nishida, and M. Nakaoka, "Deadbeat current control of LCL-filter for grid connected three-phase voltage source inverter," in *Proceedings of 2011 IEEE Ninth International Conference on Power Electronics and Drive Systems (PEDS)*, Singapore, Jan. 2011, pp. 459-467.

[11] C. N. M. Ho, V. S. P. Cheung, and H. S. H. Chung, "Constant-frequency hysteresis current control of grid-connected VSI without bandwidth

control," *IEEE Transactions on Power Electronics*, vol. 24, no. 11, pp. 2484-2495, Nov. 2009.

[12] K. Zeb, S. U. Islam, W. U. Din *et al*., "Design of fuzzy-PI and fuzzy-sliding mode controllers for single-phase two-stages grid-connected transformerless photovoltaic inverter," *Electronics*, vol. 8, no. 5, p. 520, May 2019.

[13] N. Altin and I. Sefa, "dSPACE based adaptive neuro-fuzzy controller of grid interactive inverter," *Energy Conversion and Management*, vol. 56, pp. 130-139, Dec. 2011.

[14] I. Sefa, N. Altin, S. Ozdemir *et al*., "Fuzzy PI controlled inverter for grid interactive renewable energy systems," *IET Renewable Power Generation*, vol. 9, no. 7, pp. 729-738, Apr. 2015.

[15] M. Cespedes and J. Sun, "Adaptive control of grid-connected inverters based on online grid impedance measurements," *IEEE Transactions on Sustainable Energy*, vol. 5, no. 2, pp. 516-523, Apr. 2014.

[16] X. Fu and S. Li, "Control of single-phase grid-connected converters with LCL filters using recurrent neural network and conventional control methods," *IEEE Transactions on Power Electronics*, vol. 31, no. 7, pp. 5354-5364, Jul. 2016.

[17] R. Carnieletto, D. I. Brandão, S. Suryanarayanan *et al*., "Smart grid initiative: a multifunctional-single-phase voltage source inverter," *IEEE Transactions on Industry Applications Magazine*, vol. 17, no. 5, pp. 27-35, Nov. 2009.

[18] Mathworks Inc. (2018, Dec.). SimPowerSystems—Model and simulate electrical powersystems. [Online]. Available: http: www. mathworks. com/products/simpower/

[19] D. Dong, F. Luo, X. Zhang *et al*., "Grid-interface bidirectional converter for residential DC distribution systems - part 2: AC and DC interface design with passive components minimization," *IEEE Transactions on Power Electronics*, vol. 28, no. 4, pp. 1667-1679, Apr. 2013.

[20] K. Zeb, W. Din, M. Khan *et al*., "Dynamic simulations of adaptive design approaches to control the speed of an-induction machine considering parameter uncertainties and external perturbations," *Energies*, vol. 11, no. 9, pp. 25, Sept. 2018.

Kamran Zeb received the B.Sc.E.E. and M.Sc.E.E. degrees from COMSATS Institute of Information and Technology, Abbottabad, Pakistan, in 2013 and 2016, respectively. He is currently working towards the Ph.D. degree from Pusan National University, Busan, South Korea. His research interests include power converters, control systems, renewable energies, robotics, and electrical drive.

Saif Ul Islam received the B.Sc.E.E. degree from COMSATS Institute of Information and Technology, Abbottabad, Pakistan, in 2013. He is currently working towards the M. S. E. E degree from Pusan National University, Busan, South Korea. His research interests include power electronics, control systems, renewable energies and electrical drive.

Waqar Uddin received his M.S. degree in electrical engineering from COMSATS University Islamabad, Abbottabad Campus, Pakistan, in 2016. He is currently enrolled as a Ph.D. Research Student in Pusan National University, Busan, South Korea. His research interests include modular multilevel inverter, wind energy system and AC/DC drives.

Imran Khan received the B.Sc. degree in electrical engineering from University of Engineering and Technology, Peshawar, Pakistan, in 2016. He is currently pursuing the M.S. degree from Pusan National University, Busan, South Korea. His research interests include renewables energies, power converters control design and wind turbine system.

Muhammad Ishfaq received the B.Sc. degree in electrical engineering from University of Engineering and Technology, Peshawar, Pakistan, in 2016. He is currently working towards the M.Sc. degree from Pusan National University, Busan, South Korea. His research interests include antenna design, PV thermal system, power electronics, modular multilevel converter, control system, and energy management for hybrid system.

Tiago Davi Curi Busarello received the B.S. degree from the State University of Santa Catarina, Joinville, Brazil, in 2010, and the M.S. and Ph.D. degrees from the University of Campinas, Campinas, Brazil, in 2013 and 2015, respectively. He is a member of the IEEE Industry Application Society and Power Electronics Society. His research interests include power electronics and smart grids.

Hee-Je Kim received the Ph.D. degree from Kyushu University, Fukuoka City, Japan, in 1990. At present, he is a Professor of Department of Electrical Engineering in Pusan National University, Busan, South Korea, and the group leader of Basic Research Lab. His research interests include dynamic, multi-objective, solar energy conversion, and energy storage.